ORIGINAL ARTICLE

Wernicke Encephalopathy: Typical and Atypical Findings in Alcoholics and Non-Alcoholics and Correlation with Clinical Symptoms

C. T. Arendt[1] · C. Uckermark[1] · L. Kovacheva[1] · F. Lieschke[2] · R. Golbach[3] · S. Edwin Thanarajah[4] · E. Hattingen[1] · S. Weidauer[1]

Abstract

Purpose Clinical diagnosis of Wernicke encephalopathy (WE) can be challenging due to incomplete presentation of the classical triad. The aim was to provide an update on the relevance of standard MRI and to put typical and atypical imaging findings into context with clinical features.

Methods In this two-center retrospective observational study, the local radiology information system was searched for consecutive patients with clinical or imaging suspicion of WE. Two independent raters evaluated T2-weighted imaging (WI), fluid-attenuation inversion recovery (FLAIR), diffusion WI (DWI), T2*WI and/or susceptibility WI (SWI), and contrast-enhanced (CE)-T1WI, and noted the involvement of typical (i.e., mammillary bodies (MB), periaqueductal grey (PAG), thalamus, hypothalamus, tectal plate) and atypical (all others) lesion sites. Unusual signal patterns like hemorrhages were also documented. Reported clinical features together with the diagnostic criteria of the latest guidelines of the European Federation of Neurological Societies (EFNS) were used to test for relationships with MRI biomarkers.

Results 47 patients with clinically confirmed WE were included (Jan '99–Apr '23; mean age, 53 yrs; 70% males). Interrater reliability for imaging findings was substantial ($\kappa = 0.71$), with lowest agreements for T2WI ($\kappa = 0.85$) compared to all other sequences and for PAG ($\kappa = 0.65$) compared to all other typical regions. In consensus, 77% ($n = 36/47$) of WE cases were rated MRI positive, with FLAIR ($n = 36/47$, 77%) showing the strongest relation ($\chi^2 = 47.0$; $P < 0.001$) compared to all other sequences. Microbleeds in the MB were detected in four out of ten patients who received SWI, not visible on corresponding T2*WI. Atypical findings were observed in 23% ($n = 11/47$) of cases, always alongside typical findings, in both alcoholics ($n = 9/44$, 21%) and non-alcoholics ($n = 2/3$, 67%). Isolated involvement of structures, explicitly PAG ($n = 4/36$; 11%) or MB ($n = 1/36$; 3%), was present but observed less frequently than combined lesions ($n = 31/36$; 86%). A cut-off width of 2.5 mm for the PAG on 2D axial FLAIR was established between cases and age- and sex-matched controls. An independent association was demonstrated only between short-term memory loss and changes in the MB (OR = 2.2 [95% CI: 1.1-4.5]; $P = 0.024$). In retrospect, EFNS criteria were positive (≥ 2 out of 4) in every case, but its count (range, 2–4) showed no significant ($P = 0.427$) relationship with signal changes on standard MRI.

Conclusion The proposed sequence protocol (FLAIR, DWI, SWI and T1WI+CE) yielded good detection rates for neuroradiological findings in WE, with SWI showing microbleeds in the MB with superior detectability. However, false negative results in about a quarter of cases underline the importance of neurological alertness for the diagnosis. Awareness of atypical MRI findings should be raised, not only in non-alcoholics. There is limited correlation between clinical signs and standard MRI biomarkers.

Keywords Magnetic resonance imaging · Wernicke Encephalopathy · Thiamine Deficiency · Alcoholism · Malnutrition

✉ C. T. Arendt
arendt@med.uni-frankfurt.de

1 Institute of Neuroradiology, University Hospital Frankfurt, Goethe University, Frankfurt/Main, Germany

2 Department of Neurology, University Hospital Frankfurt, Goethe University, Frankfurt am Main, Germany

3 Institute of Biostatistics and Mathematical Modeling, University Hospital Frankfurt, Goethe University, Frankfurt am Main, Germany

4 Department for Psychiatry, Psychosomatic Medicine and Psychotherapy, University Hospital Frankfurt, Goethe University, Frankfurt am Main, Germany

Abbreviations

CE	Contrast-enhanced
EFNS	European Federation of Neurological Societies
FLAIR	Fluid-attenuated inversion recovery
MB	Mammillary bodies
PAG	Periaqueductal grey
WE	Wernicke encephalopathy
WI	Weighted imaging

Introduction

German neurologist Carl Wernicke defined 'acute superior hemorrhagic polioencephalitis' from three cases, although similar findings were first reported by French ophthalmologist Alphonse-Charles Gayet [1, 2]. Subsequently, Wernicke encephalopathy (WE) has been recognized as a severe neurological condition that is caused by a deficiency of thiamine (vitamin B1). The classical clinical triad of acute WE encompasses oculomotor disturbances, cerebellar dysfunction with prominent ataxia, and altered mental state or mild cognitive impairment [3]. Most importantly, the diagnosis of WE can be very challenging due to incomplete or variable symptomatology or physician's unawareness of them [4]. Untreated WE may lead to Korsakoff psychosis, an irreversible neurological disorder characterized by severe anterograde amnesia, or even death may occur [5–7].

Thiamine is crucial for the Krebs and pentose phosphate pathways, maintaining cellular integrity [8] primarily in regions like the medial thalamic nuclei, hypothalami, mammillary bodies (MB), midbrain tectum, and periaqueductal grey (PAG) [9, 10]. Low thiamine levels correlate with diffusion restrictions of water molecules, indicative of early cytotoxic edema and subsequent vasogenic changes, including blood-brain barrier leakage [11, 12]. These changes produce symmetric, hyperintense signals on diffusion-weighted images (DWI) and/or T2WI/FLAIR, and enhancement on contrast-enhanced(CE)-T1WI [13–15]. Acute WE can also feature petechial hemorrhages, evolving into capillary sprouting and atrophy, detectable with susceptibility WI (SWI) as areas of signal loss [1, 16–19].

Early disease detection and treatment by vitamin B1 supplementation are crucial for the prognosis of potentially reversible WE. The implementation of the 2010 EFNS (European Federation of Neurological Societies) guidelines for diagnosis, therapy, and prevention of WE has improved its detection rate to up to 85% based on clinical features [20]. The diagnosis relies on the presence of at least two out of four clinical parameters, i.e., dietary deficiencies, oculomotor signs, cerebellar dysfunction, and either altered mental state or mild memory impairment [20]. Albeit imaging findings are not mandatorily required, MRI adds value in confirming the diagnosis, especially in cases with incomplete neurological presentation [13, 21]. It is of note that standard MRI has a reported low sensitivity of 53% in the 2010 EFNS guidelines. Thus, the absence of lesions does not exclude WE, but it does exhibit a high specificity of up to 93% [20, 22]. Moreover, atypical neuroimaging findings need to be acknowledged [23–30].

The purpose of the present study was to evaluate the prevalences of typical and atypical neuroradiological findings in patients with WE using standard MRI with continuously reliable scanning protocols and to correlate them with clinical features.

Materials and Methods

Research Design and Subjects

This retrospective study was conducted at two centers of the University Hospital Frankfurt of the Goethe University, Germany, and was approved by the local ethics committee (2023–1296) with a waiver for informed consent. In center A and B, the radiology information system (RIS) was used to search for patients with WE using specific key words in the clinical information and radiology reports. Only patients aged ≥18 years who had undergone an MR examination were included. The final cohort was determined based on clinical and radiological criteria by reviewing the diagnosis on medical reports from the clinical information system and the image quality of the institutional MRI, respectively—i.e., patients with other causative diseases for the underlying symptoms or with images of low quality (e.g., motion artifacts) were excluded. For a subgroup analysis (see below), the RIS of center A was searched for a control cohort without WE, and without any other neurological or psychiatric precondition or detected structural changes on brain MRI. These participants were consecutively enrolled and matched for sex, age, and type of scanner, the latter to account for scanner-dependent contrast variations in the MR images. Baseline characteristics of all subjects were collected from the local clinical information system, and number of positive criteria (range, 0–4) according to the 2010 EFNS guidelines [20] was noted a posteriori.

MR Imaging Analysis

Datasets were acquired on five different MR scanners with a magnetic field strength of 3T (MAGNETOM Skyra (a) & Verio (b), Siemens Healthineers, Germany) and 1.5T (MAGNETOM Symphony (c) & Aera (d), Siemens Healthineers, Germany; Achieva dStream (e), Philips, Netherlands). Two experienced neuroradiologists (S.W. and

C.T.A.) analyzed the following sequences, if available: (1) T2WI, (2) FLAIR, (3) DWI, (4) SWI, (5) T2*WI, and (6) T1WI before and after the intravenous application of a body weight-adapted gadolinium-based contrast agent. In ascending order, technical parameters for these sequences (1–6) on each scanner (a/b/c/d/e) are detailed as follows: (1) slice thickness (ST), 5/5/6/5/5 mm, time of repetition (TR), 4980/4980/4000/4700/5762 ms, time of echo (TE), 92/92/103/111/110 ms, flip angle (FA), 150/150/150/180/90°, matrix (mtx), 336×448/336×448/448×512/224×256/672×672; (2) ST, 4/5/6/5/5 mm, TR, 8500/6630/8500/9000/11,000 ms, TE, 81/131/125/86/140 ms, FA, 50/130/150/150/90°, mtx, 280×320/200×320/268×320/280×320/576×576, time of inversion, 2440/2140/2500/2440/2800 ms; (3) ST, 5/5/5/5/5 mm, TR, 3800/4900/3200/5190/3247 ms, TE, 95/88/94/60/75 ms, FA, 90/90/90/180/90°, mtx, 384×384/130×130/128×128/160×160/256×256, b-values of 0, 500, and 1,000 s/mm²; (4) ST, 1.5/1.5/–/2/2 mm, TR, 27/27/–/49/52 ms, TE, 20/20/–/40/0 ms, FA, 15/15/–/15/20°, mtx, 464×512/192×256/–/232×256/672×672; (5) ST, 5/5/6/–/5 mm, TR, 631/631/657/–/530 ms, TE, 20/20/26/–/14 ms, FA, 20/20/20/–/18°, mtx, 432×512/432×512/416×512/–/320×320; (6) ST, 5/5/6/5/5 mm, TR, 600/662/485/550/664 ms, TE, 13/12/14/9/14 ms, FA, 70/70/90/90/67°, mtx, 288×384/288×384/448×512/320×320/512×512. Except for the three-dimensional image acquisition of SWI, all other sequences were acquired in a two-dimensional way. The field of view for all the sequences encompassed the entire head.

For each sequence and topographic location, both raters independently assessed areas with well-defined hyperintensities on T2WI and FLAIR, signal loss on SWI with blood-equivalent signals on the corresponding phase map (i.e., hemorrhage, including microbleeds defined as a size of <5 mm diameter), signal loss on T2*WI (i.e., hemorrhage, insensitive to smaller microbleeds), hyperintense signal changes on DWI at a b-value of 1000 s/mm² together with reduced ADC values on the corresponding map (i.e., diffusion restriction) and contrast-enhancement on CE-T1WI (i.e., disrupted blood-brain barrier). Typical imaging features of WE were defined as the presence of at least one pathological symmetric signal change located in the most commonly described anatomical structures in scientific literature [9, 10, 30], namely the thalami (esp. medial nuclei), hypothalami, MB, tectal plate (esp. inferior colliculus), and PAG. Involvement of atypical regions (i.e., all except those mentioned above) [11, 12, 21–28], or atypical presentations (i.e., space-occupying lesions with or without hemorrhage) were additionally documented. In cases of any discrepancy regarding the ratings of sequences, or of involvement of typical and atypical regions, decision-making was performed in a consensus reading.

Furthermore, all available axial FLAIR images of each participant in the patient and control cohort were scrolled down to the mid-lower level of the midbrain to measure the largest width of the hyperintense PAG between the medial border adjacent to the aqueduct and the lateral border. Measurements were rounded to the nearest millimeter as appropriate. In addition, the shape of the FLAIR hyperintense signal changes around the PAG were classified as either triangular or circular.
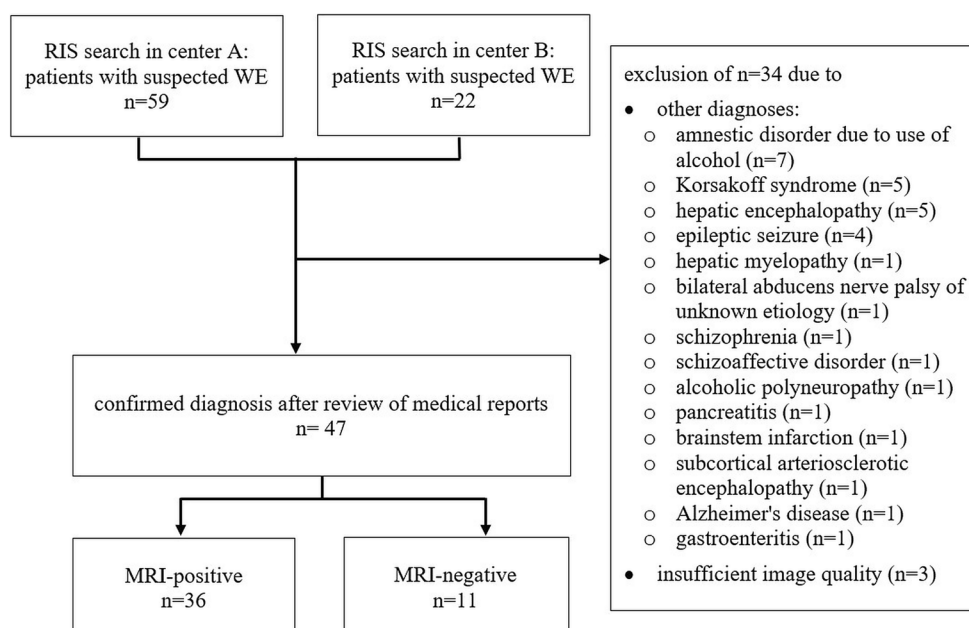
Statistical Analysis

All computations were performed using a structural equation modeling software (IBM SPSS Statistics, Armonk/NY, USA, version 29.0). Variables are presented as absolute frequencies, percentages, and proportions, means with standard deviations (SD), or medians with first and third quartiles (Q1–Q3), as applicable. The significance level α was set to 5%, and P-values <0.05 were considered statistically significant. 95% confidence intervals (CI) of results are reported wherever appropriate. To test for differences or relationships, either parametric (independent two-sided t-test) or non-parametric (Fisher's exact, Pearson's χ^2, Wilcoxon-Mann-Whitney U test) statistical tests were performed, depending on the data distribution as determined by the Lilliefors-corrected Kolmogorov-Smirnov test. Corrections for the alpha error due to multiple testing were not performed because of the descriptive nature of the research design. Binary logistic regression analysis with backward elimination method (Wald) was used to determine independent relationships between clinical symptoms and imaging findings. The maximum likelihood estimation method was used to obtain the most likely mean and standard deviation of the underlying normal distribution for the normal width of the PAG. In this subgroup analysis, MRI datasets from controls (intended for a diagnostic workup within the scope of excluding brain metastases) were included consecutively for each scanner type, provided that motion-free, axial 2D FLAIR was acquired. Interrater agreement was measured using Cohen's κ, with the following grading to assess the strength of agreement: κ = 0, poor; κ = 0.01–0.20, slight; κ = 0.21–0.40, fair; κ = 0.41–0.60, moderate; κ = 0.61–0.80, substantial; κ = 0.81–1.00, almost perfect.

Results

Study Participants

The final patient cohort comprised 47 subjects with clinically confirmed WE, with MR examinations conducted between January 1999 and May 2023. The mean age was 53.0 ± 9.8 yrs (range, 28–71 yrs), and the group predomi-

Fig. 1 Flow chart of the study cohort design. (*RIS* radiology information system)

RIS search in center A: patients with suspected WE n=59

RIS search in center B: patients with suspected WE n=22

exclusion of n=34 due to

- other diagnoses:
  - amnestic disorder due to use of alcohol (n=7)
  - Korsakoff syndrome (n=5)
  - hepatic encephalopathy (n=5)
  - epileptic seizure (n=4)
  - hepatic myelopathy (n=1)
  - bilateral abducens nerve palsy of unknown etiology (n=1)
  - schizophrenia (n=1)
  - schizoaffective disorder (n=1)
  - alcoholic polyneuropathy (n=1)
  - pancreatitis (n=1)
  - brainstem infarction (n=1)
  - subcortical arteriosclerotic encephalopathy (n=1)
  - Alzheimer's disease (n=1)
  - gastroenteritis (n=1)
- insufficient image quality (n=3)

confirmed diagnosis after review of medical reports n= 47

MRI-positive n=36

MRI-negative n=11

nantly consisted of men ($n=33/47$, 70%). History of alcohol use disorder was a frequent cause for WE ($n=44/47$, 94%). Other causes were hunger strike ($n=1$), anorexia nervosa ($n=1$), and gastrectomy due to primary carcinoma ($n=1$), each accounting for 2% of the cases. Figure 1 indicates a flow chart of the study cohort design.

Imaging Protocols and Interrater Agreements

Out of 47 cases, 36 (77%) were finally rated as MRI positive. Interrater agreement was substantial ($\kappa=0.71$) for the final imaging-guided diagnosis of WE. FLAIR und T2WI were included in all sequence protocols (both $n=47/47$, 100%), whereas CE-T1WI ($n=42/47$; 89%), DWI ($n=35/47$, 75%), T2*WI ($n=27/47$; 58%) and SWI ($n=10/47$; 21%) were not. Both hemosiderin-sensitive sequences were acquired in seven of the 47 datasets (15%) during the same examination. The consensus reading emphasized that discrepancies between raters led to disagreement in five cases ($n=5/47$, 11%) for the final diagnosis of WE. The lowest agreements were detected for the presence/absence of signal changes in T2WI ($\kappa=0.85$) compared to all other sequences, and for signal changes in the PAG ($\kappa=0.65$) compared to all other typical regions. One case was determined as MRI negative due to a misinterpretation of contrast enhancement of the tectal plate, and four cases were diagnosed as MRI positive due to initially undetected pathological circular widening of FLAIR hyperintense PAG.

Typical Neuroimaging Findings

In decreasing order, involvement of typical locations was as follows: medial thalamic nuclei, $n=24/47$ (51%); PAG, $n=22/47$ (47%); MB, $n=16/47$ (34%); tectal plate, $n=13/47$ (28%); and hypothalamus, $n=7/47$ (15%) (see Table 1). In all these areas with positive diagnoses, the hyperintensities detected on FLAIR images ($n=36/47$, 77%) were stronger associated with MRI positive cases ($\chi^2=47.0$; $P<0.001$) than those on T2WI ($n=17/47$; 36%; $\chi^2=8.1$; $P=0.004$), indicating that FLAIR images were crucial for diag-

Table 1 Summary of typical and atypical lesion sites with signal changes identified in a cohort of 47 patients with WE

| Lesion sites	Numbers (%)
Typical	
Total	36 (77)
Medial thalamic nuclei	24 (51)
Periaqueductal grey	22 (47)
Mammillary bodies	16 (34)
Tectal plate	13 (28)
Hypothalamus	7 (15)
Atypical	
Total	11 (23)
Fornices	4 (9)
Cerebellar Peduncles	2 (4)
Cerebral Cortices	1 (2)
Internal Capsules	1 (2)
Optic Pathway	1 (2)
Mammillo-tegmental/habenulo-interpedunclar tract	1 (2)
Brainstem/cranial nerve nuclei	1 (2)
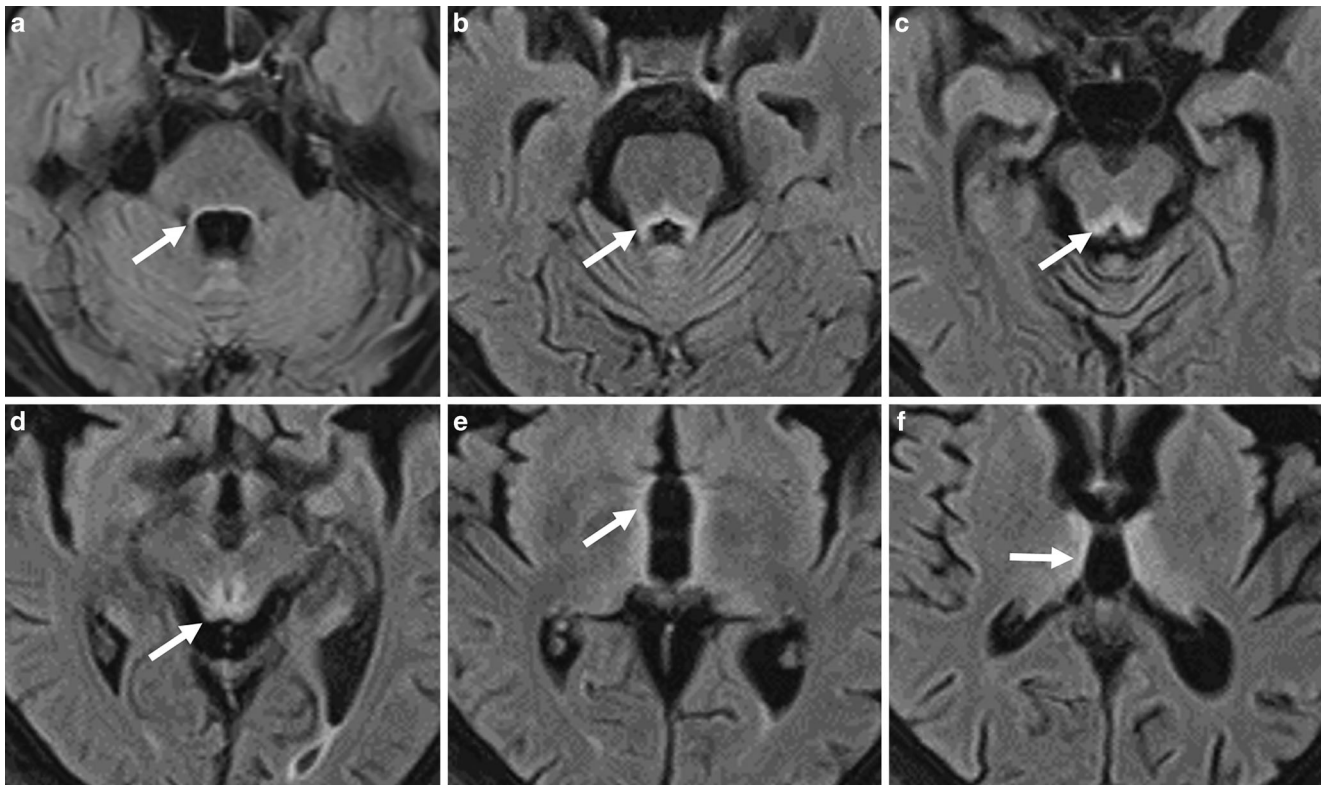
Fig. 2 Characteristic brainstem and thalamic involvement in a 56-year-old female alcoholic with Wernicke encephalopathy. Hyperintense signal changes of the pontine tegmentum (**a, b**; arrow), the superior cerebellar peduncle (**b**, arrow), the quadrigeminal plate and the periaqueductal grey matter (**c, d**; arrow), paramedian thalamic nuclei (**e**, arrow), hypothalamus (**e**) and pulvinar of the thalamus (**f**, arrow); **a–f** axial fluid-attenuated inversion recovery

nosing WE. Concomitant contrast enhancement ($n = 18/47$, 38%), diffusion restriction ($n = 12/47$, 26%), or presence of hemosiderin ($n = 7/47$, 15%) were also observed. Figures 2, 3, 4 and 5 depict four instructive cases with predominantly typical neuroimaging findings. Of the seven patients with signal loss on hemosiderin-sensitive sequences, four demonstrated microbleeds in the MB on SWI, as opposed to simultaneously acquired T2*WI (see Fig. 5). Isolated anatomical involvement was present only in PAG ($n = 4/36$, 11%) or MB ($n = 1/36$; 3%), but was less frequently observed ($\chi^2 = 47.0$; $P < 0.001$) than combined lesions ($n = 31/36$; 86%).

Atypical Neuroimaging Findings

Atypical findings were observed in 23% of cases ($n = 11/47$), showing symmetric signal changes in the following locations: fornix, $n = 4/47$ (9%), cerebellar peduncle, $n = 2/47$ (4%), cerebral cortex, $n = 1/47$ (2%); internal capsule, $n = 1/47$ (2%); visual pathway, $n = 1/47$ (2%); junction area of the mammillo-tegmental and habenulo-interpeduncular tract, $n = 1/47$ (2%) and the brainstem/cranial nerve nuclei, $n = 1/47$ (2%) (see Table 1). Two out of three (67%) non-alcoholic and four out of 44 (9%) alcoholic patients with

WE showed an involvement of atypical lesion sites (Figs. 6, 7 and 8).

While almost all these findings were present on FLAIR images, one case involving the fornix showed clear signal alterations only on DWI. All these changes were only present in addition to the involvement of typical brain areas. Three patients ($n = 3/47$, 6%) displayed more extensive hyperintense lesions with a space-occupying pattern on FLAIR/T2WI and concomitant macrohemorrhages on T2*WI, either in the thalami ($n = 1/47$, 2%) and brainstem ($n = 1/47$, 2%), or combined in the PAG, tectal plate and thalami with rupture into the ventricles ($n = 1/47$, 2%) (Figs. 9, 10 and 11).

Matched-Pair Analysis of the Periaqueductal Grey

32 controls (mean age, 52.8 ± 9.0 yrs; age range, 30–86 yrs; sex, 72% males) were included in the subgroup analysis and matched with the patient group (age, $P = 0.931$; sex, $P = 0.685$; scanner-type, $P = 1.000$). None of these subjects showed signal changes suggestive of WE, according to both raters. To determine a normal range of values for the maximal width of the PAG on axial FLAIR, an estimated maximum likelihood mean with one SD of 1.45 ± 0.16 mm for
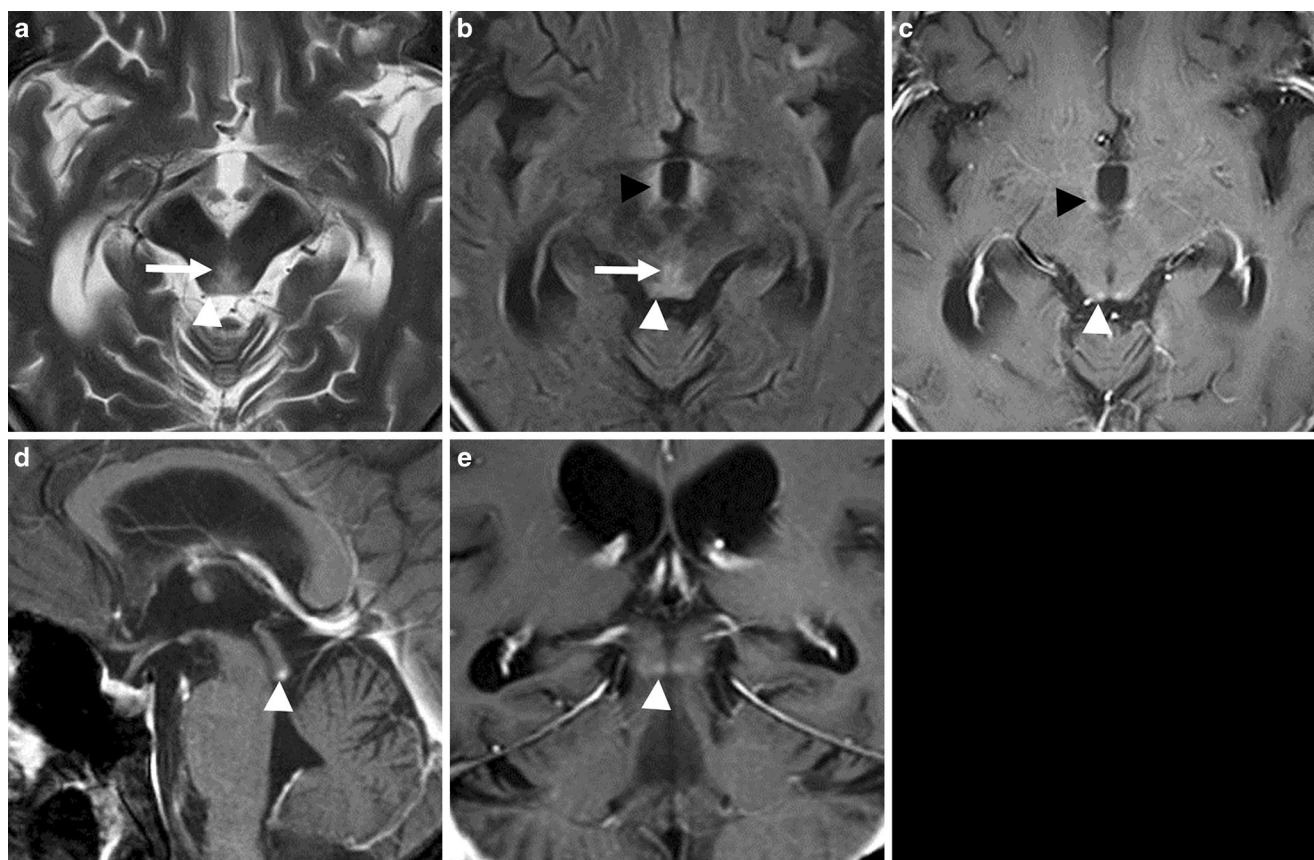
Fig. 3 Hyperintense signal changes of the periaqueductal grey (**a, b**; arrow) and the inferior colliculus (**a, b**; white arrowhead) with distinct enhancement on contrast-enhanced (CE) T1-weighted images (WI) (**c–e**; white arrowhead) in a 66-year-old male alcoholic. Hyperintense lesion in the hypothalamus (**b**, black arrowhead; axial fluid-attenuated inversion recovery) and contrast enhancement of the mammillary bodies (**c**, black arrowhead; axial CE-T1WI)

the underlying normal distribution was obtained, considering that measurements were rounded to whole numbers (range, 1–4 mm). Consequently, a 95% reference interval of 1.14 to 1.76 mm was established for healthy controls, i.e., 1 to 2 mm after rounding the numbers. Consecutively, a cut-off value of 2.5 mm (i.e., rounded up to 3 mm) was used for pathological enlargement of the PAG. As two patients with visually assessed positive finding of the PAG presented values for the maximal width of rounded 2 mm in the quantitative analysis, both were retrospectively considered as MRI negative for this area, resulting in a final number of $n = 20/47$ (43%) cases of PAG involvement. However, these two patients had additional thalamic lesions suggestive of WE, thus the final number of MRI positive cases was not affected. The patterns were triangular in 32% ($n = 15/47$) and circular in 11% ($n = 5/47$) of cases (Fig. 12).

Associations of Clinical and Imaging Features

Table 2 displays the frequencies of neurological symptoms related to the classical triad, as noted in the medical reports. All patients, both with and without positive findings on MRI, ultimately met the 2010 EFNS diagnosis criteria for WE ($n = 47/47$, with $\geq 2/4$ criteria met). Additionally, there was no significant relation ($P = 0.427$) observed between the number of positive clinical criteria (0, $n = 0/47$, 0%; 1, $n = 0/47$, 0%; 2, $n = 2/47$; 4.3%; 3, $n = 19/47$, 40.4%; 4, $n = 26/47$, 55.3%) and MRI-based diagnosis. Significant correlations between clinical symptoms and region-based imaging findings were found only between short-term memory loss and changes in the MB ($\chi^2 = 7.6$; $P = 0.010$) or fornix ($\chi^2 = 6.2$; $P = 0.024$), and between cognitive impairment and the PAG ($\chi^2 = 7.6$; $P = 0.010$). An independent association was demonstrated only between short-term memory loss and changes in the MB (OR = 2.2 [95% CI: 1.1–4.5]; $P = 0.024$).

Discussion

This two-center, retrospective, observational study emphasizes the role of standard MRI besides the clinical workup in patients with WE, and suggests a sequence protocol together with an approach to look for typical [12, 13, 21] and
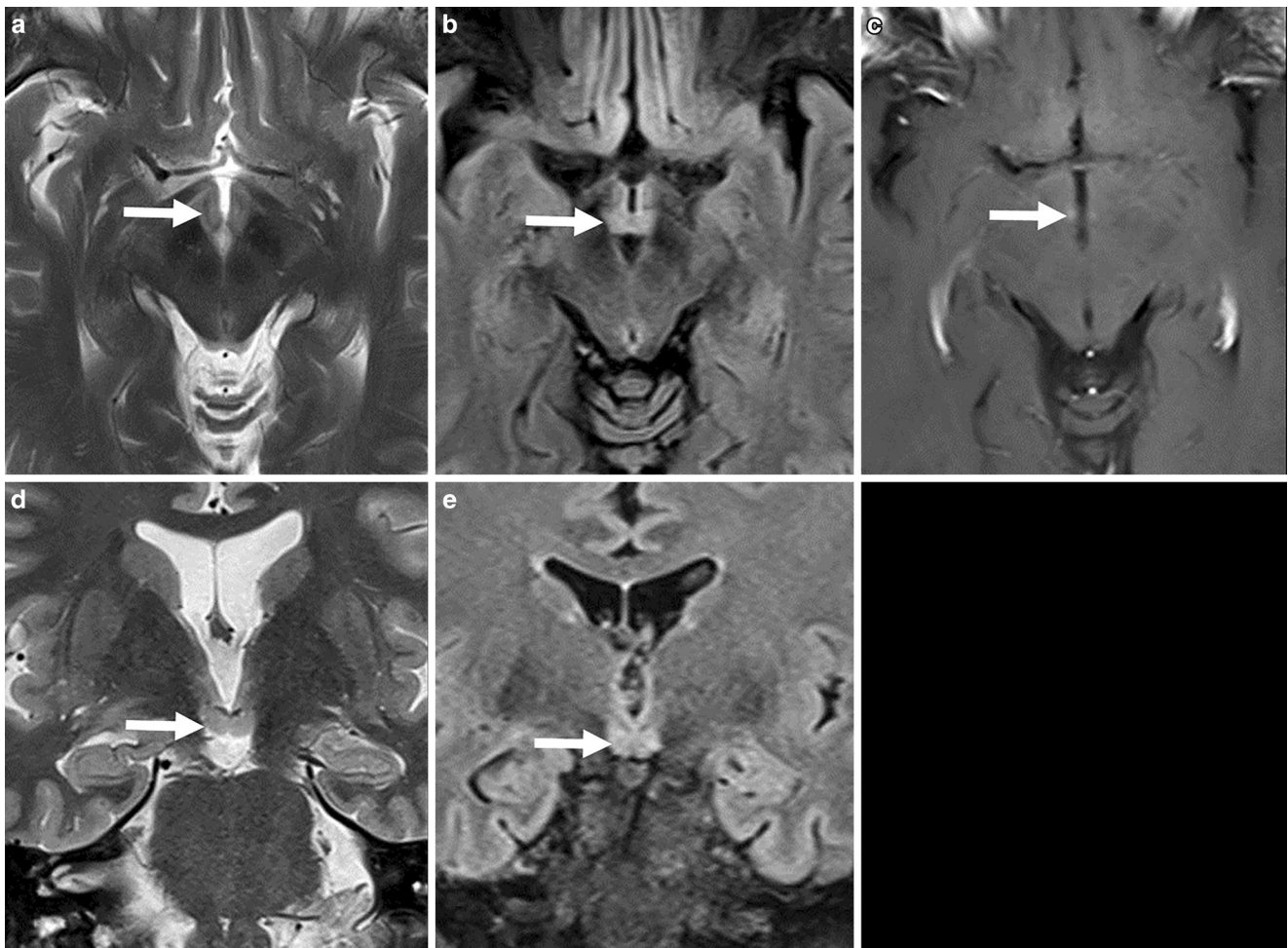
Fig. 4 Swelling with hyperintense signal changes of the mammillary bodies on T2-weighted images (WI) and fluid-attenuated inversion recovery images (**a, b** axial; **d, e** coronal; arrow) with slight enhancement on axial contrast-enhanced T1WI (**c**, arrow) in a 63-year-old female non-alcoholic. Note additional hyperintense signal changes of the hypothalamus (**a**, **b**, **d**, **e**)

atypical [23–30] neuroradiological findings (Fig. 13). The results of this study can be summarized as follows. Neuroradiological awareness should be raised regarding the high prevalence of atypical MRI findings [23–30], which include locations other than the thalami, hypothalami, MB, PAG, and tectal plate, as well as manifestations such as bleedings with or without perifocal edema, not only present in non-alcoholics as previously stated [30]. FLAIR, DWI, CE-T1WI and SWI were the most important sequences, the latter demonstrating a higher detectability for microbleeds in the MB compared to T2*WI [17, 19]. Matched-pair analyses revealed that the PAG could be defined as pathologically enlarged using a minimal cut-off width of rounded up 3 mm. Taken together, neuroradiologists that used dedicated diagnostic MRI sequences could yield high positive detection rates of WE, but false negative results remained a limitation for the diagnosis in approximately a quarter of cases [21]. Inconsistency of MRI protocols, which is mainly due to the very large retrospective timeframe of this bicentric

study, and the omission of volumetric analyses introduce the main limitations that may affect the outcome of the diagnostic accuracy and comparability of the results. From a clinical point of view, all patients met retrospectively the 2010 EFNS criteria [20], but the number of positive criteria did not correlate with the extent of neuroradiological signatures. Whilst only short-term memory loss showed an independent association with the radiographic affection of the MB, all other clinical signs and standard MRI biomarkers did not.

The discovery of vitamins is partly credited to Dutch physician Christiaan Eijkman, who identified the first disease from the group of avitaminoses. He noted that chickens developed neurological disorders when fed solely on polished rice, which lacks the thiamine-rich outer layer [31]. The state of a severe lack of thiamine is known as beriberi, which can be classified into a wet form affecting the cardiovascular system and a dry form impacting the nervous system. WE and Korsakoff psychosis, manifesta-
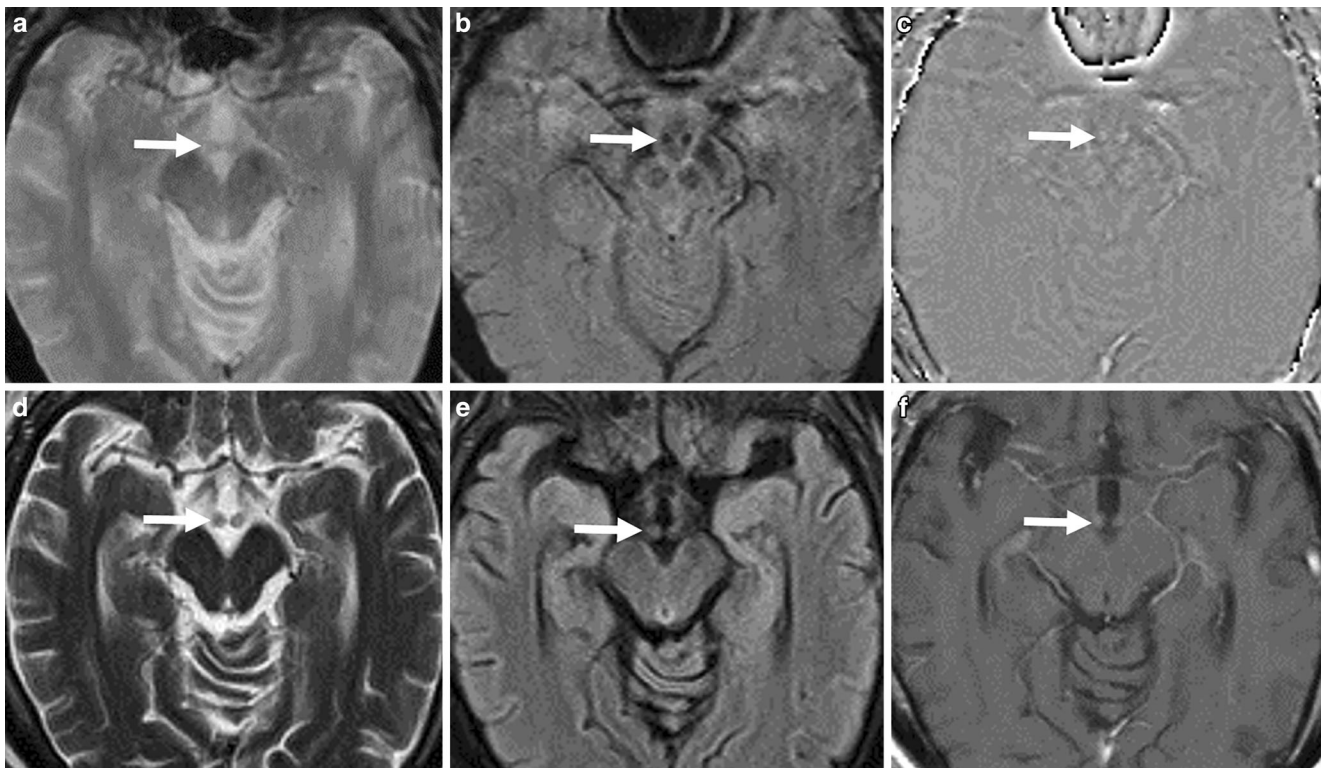
Fig. 5 Symmetrical signal loss in the mammillary bodies (MB) due to microhemorrhages (**b**, arrow; axial susceptibilit- weighted imaging (SWI)) with phase shifting, indicating paramagnetic effects of iron (**c**, arrow; SWI-phase map), not visible on T2*WI (**a**, arrow). Axial T2WI (**d**, arrow) and fluid-attenuated inversion recovery images (**e**, arrow) showing inhomogeneous hyperintense signal changes of the MB with slight enhancement on axial contrast-enhanced T1WI (**f**, arrow) in this 53-year-old male alcoholic
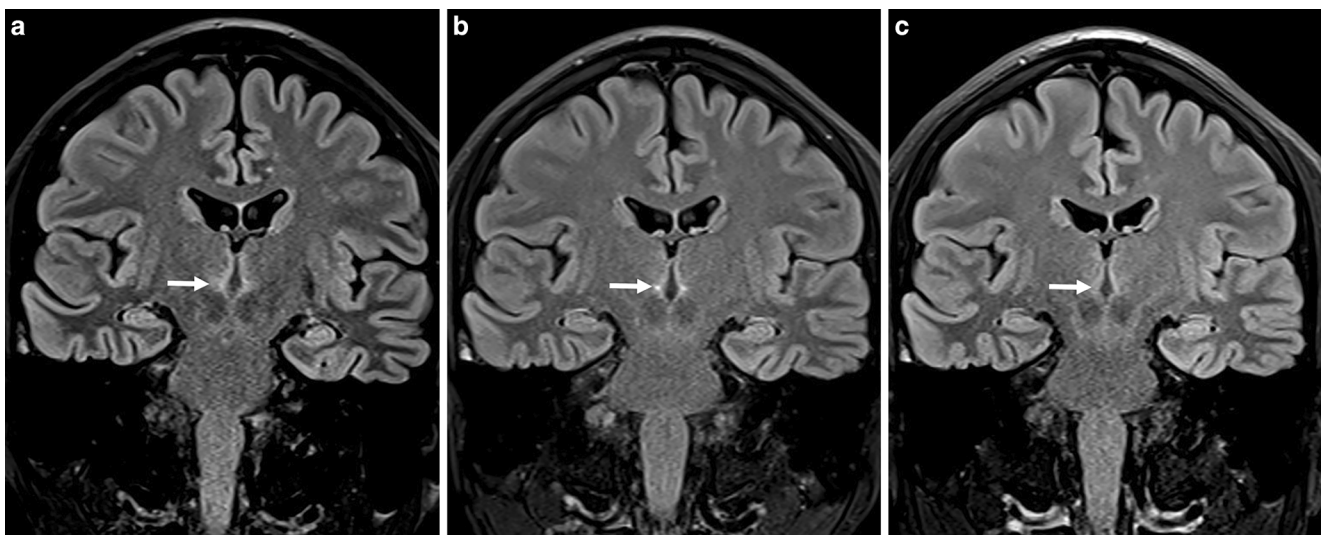
Fig. 6 Circumscribed possible involvement of the junction area of the mammillo-tegmental and the habenulo-interpeduncular tract (directly above the red nucleus) in a 28-year-old male non-alcoholic on a hunger strike (**a**, arrow; coronal fluid-attenuated inversion recovery images). Follow-up MRI 22 days later (**b**) disclosed progressive punctuate hyperintense signal changes (arrow) despite vitamin B1 substitution; **c** incomplete lesion regression (arrow) on day 101 after resumed food intake in the meantime

tions of dry beriberi, are predominantly caused by a chronic abuse of alcohol, which provides high calories but low nutrients. However, they can also occur in association with anorexia nervosa, hyperemesis gravidarum, hunger strike, bariatric surgery, and inflammatory or malignant diseases of the gastrointestinal tract [13, 14, 21, 32–34]. This observation is corroborated by the current study, where hunger
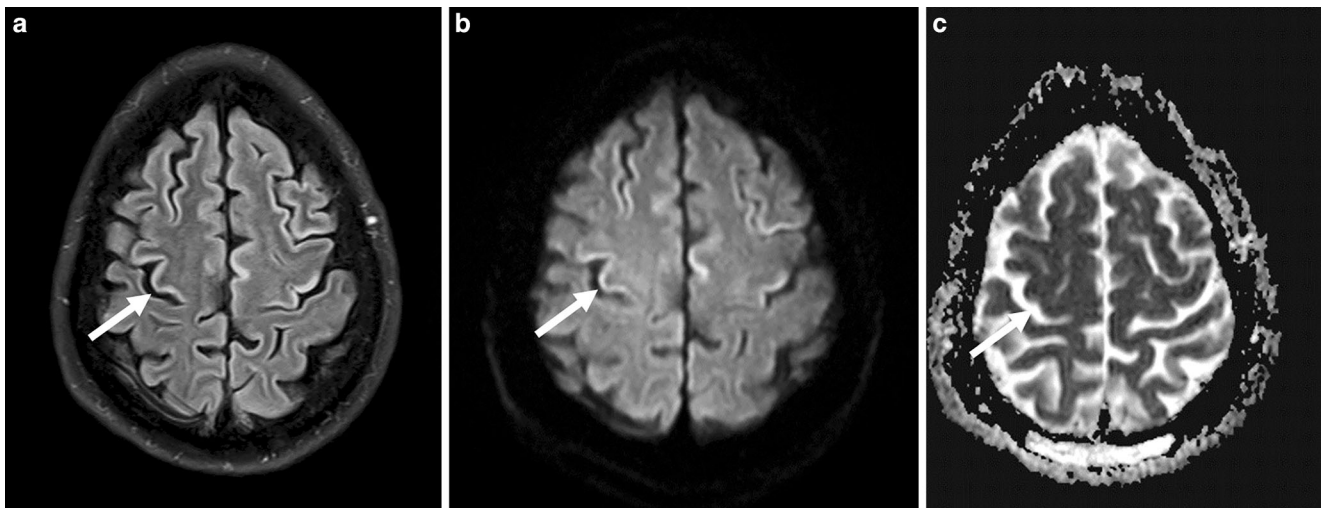
Fig. 7 Involvement of the frontal and precentral cortical grey matter with hyperintense signal conversion on axial fluid-attenuated inversion recovery images (**a**, arrow); **b,c** diffusion-weighted imaging, b = 1000 s/mm^2 (**b**) with normal apparent diffusion coefficient (ADC) value on ADC maps (**c**, arrow) in a 49-year-old female alcoholic

Fig. 8 Involvement of both fornices with hyperintense signal changes (**a**, arrow; axial fluid-attenuated inversion recovery; arrowhead: choroid plexus) with distinct enhancement on contrast-enhanced T1-weighted images (WI) (**b** before, **c** after administration of contrast agent, arrow; arrowhead: choroid plexus) in a 53-year-old male non-alcoholic; **d,e** diffusion-WI disclosing restricted diffusion (**d** b = 1000 s/mm^2; **e** apparent diffusion coefficient map; mean (SD): 0.61 (0.16) × 10^{-3} mm^2/s, black and white arrow. Control subject: mean (SD) 0.76 (0.11) × 10^{-3} mm^2/s)
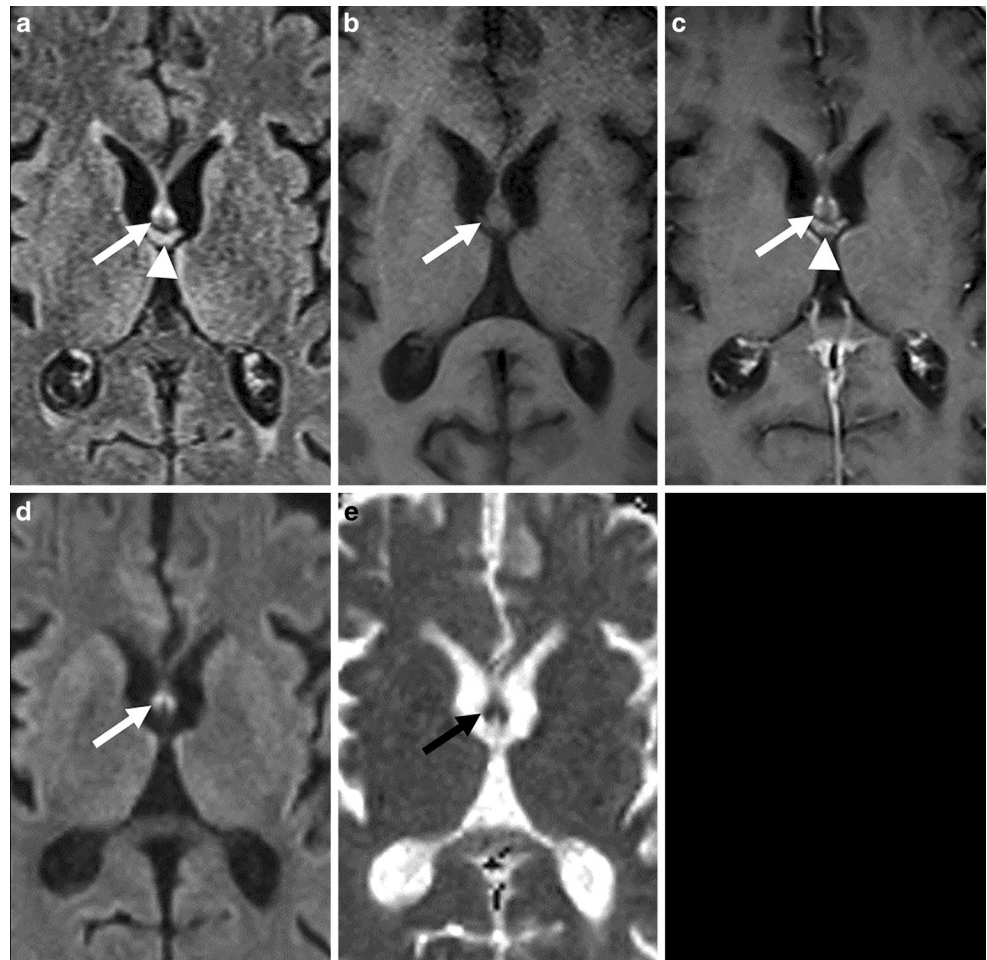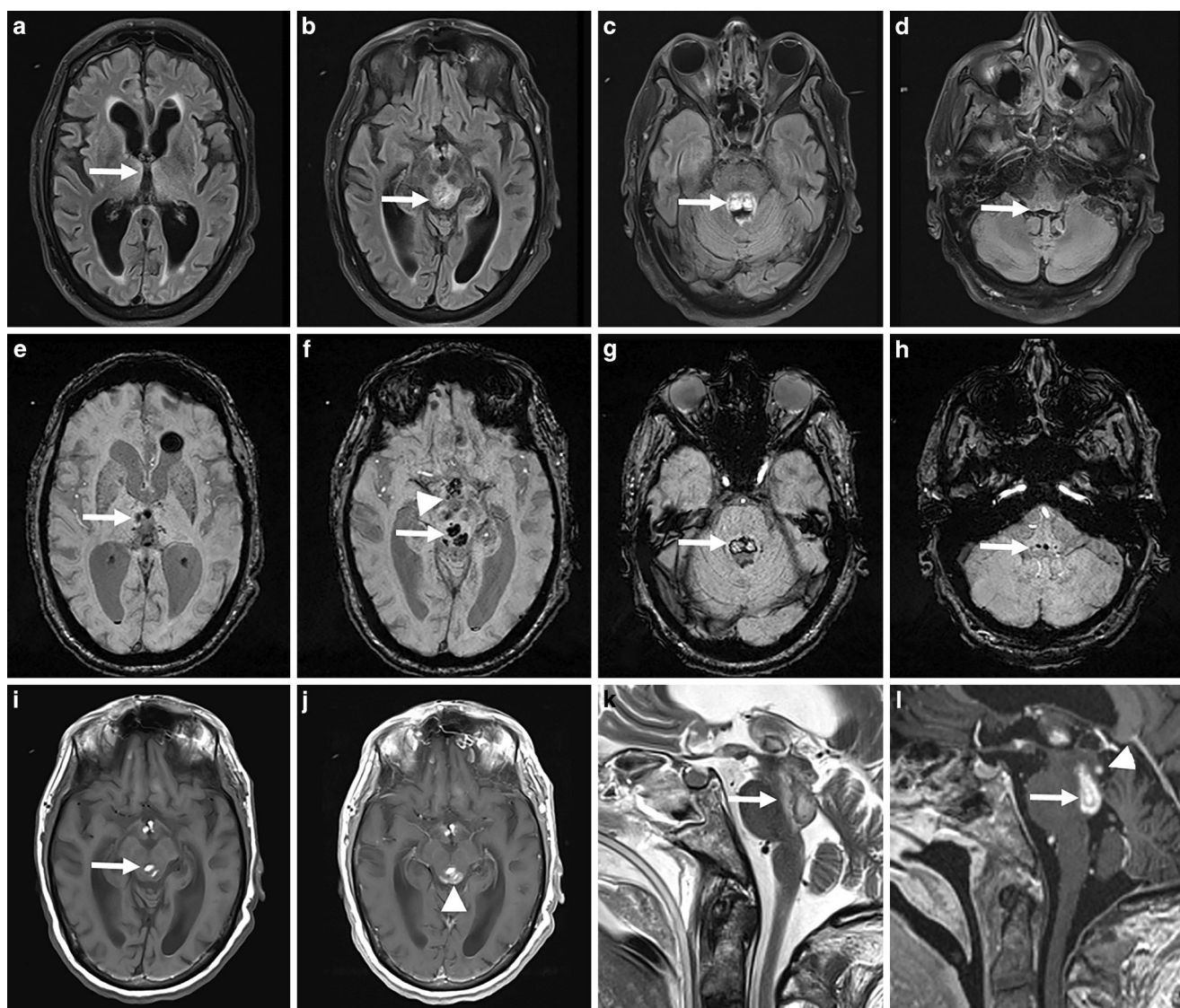
Fig. 9 Distinct hemorrhages in the paramedian thalamic nuclei (**e**, arrow), the periaqueductal grey and the quadrigeminal plate (**f**, arrow), the mammillary bodies (**f**, arrowhead) and the pontine tegmentum (**g, h**, arrow) with inhomogeneous signal loss on susceptibility-weighted imaging (SWI) in a 61-year-old male alcoholic. **a–d** corresponding hyperintense lesions on axial fluid-attenuated inversion recovery images (arrow); **k** sag. T2WI (arrow). Enhancement of the inferior colliculus on contrast-enhanced T1WI (**j, l**, arrowhead) and partially hyperintense lesions on T1WI (**i, l**, arrow). Note additional intraventricular clots

strike, anorexia nervosa and gastrectomy were rare (6 %) but present factors alongside alcoholism (94 %) [32–34].

Diagnostic imaging most commonly revealed signal changes in regions near the third ventricle and the cerebral aqueduct, i.e., involved the medial thalamic nuclei, hypothalami, MB, midbrain tectum, and PAG [13, 14, 21, 22]. Multiple imaging studies and case reports have described the following atypical lesion sites: cerebral cortices [26, 35], striate nuclei [23, 26, 28, 36–38], internal capsules [38, 39], amygdalae [29], corpus callosum (splenium, in particular) [24, 38, 40], optic pathways [39, 41, 42], fornices [29, 43, 44], cerebral peduncles [38], red nuclei [24, 25], substantia nigra [45], brainstem/cranial nerve nuclei (bulbo-

pontine tegmentum, in particular) [14, 25, 27, 28, 36–38, 45, 46], cerebellar peduncles [47], cerebellar hemispheres [14, 27, 28, 48, 49], dentate nuclei [14, 24, 25, 28, 45], and the vermis [44, 49]. Like the results of Zuccoli et al. [30], who studied the largest number of subjects with WE ($n =$ 56) to date, atypical lesion sites always co-occurred with typical regions in our study. However, that study reported these atypical findings only in non-alcoholic patients with WE. In contrast, approximately 10% of alcoholic patients in our cohort ($n = 4/44$) also showed symmetric changes of signal intensities in more unusual locations (see Table 1) such as the cerebral cortex, the internal capsule, the visual pathway, the cerebellar peduncle, and/or the brainstem/
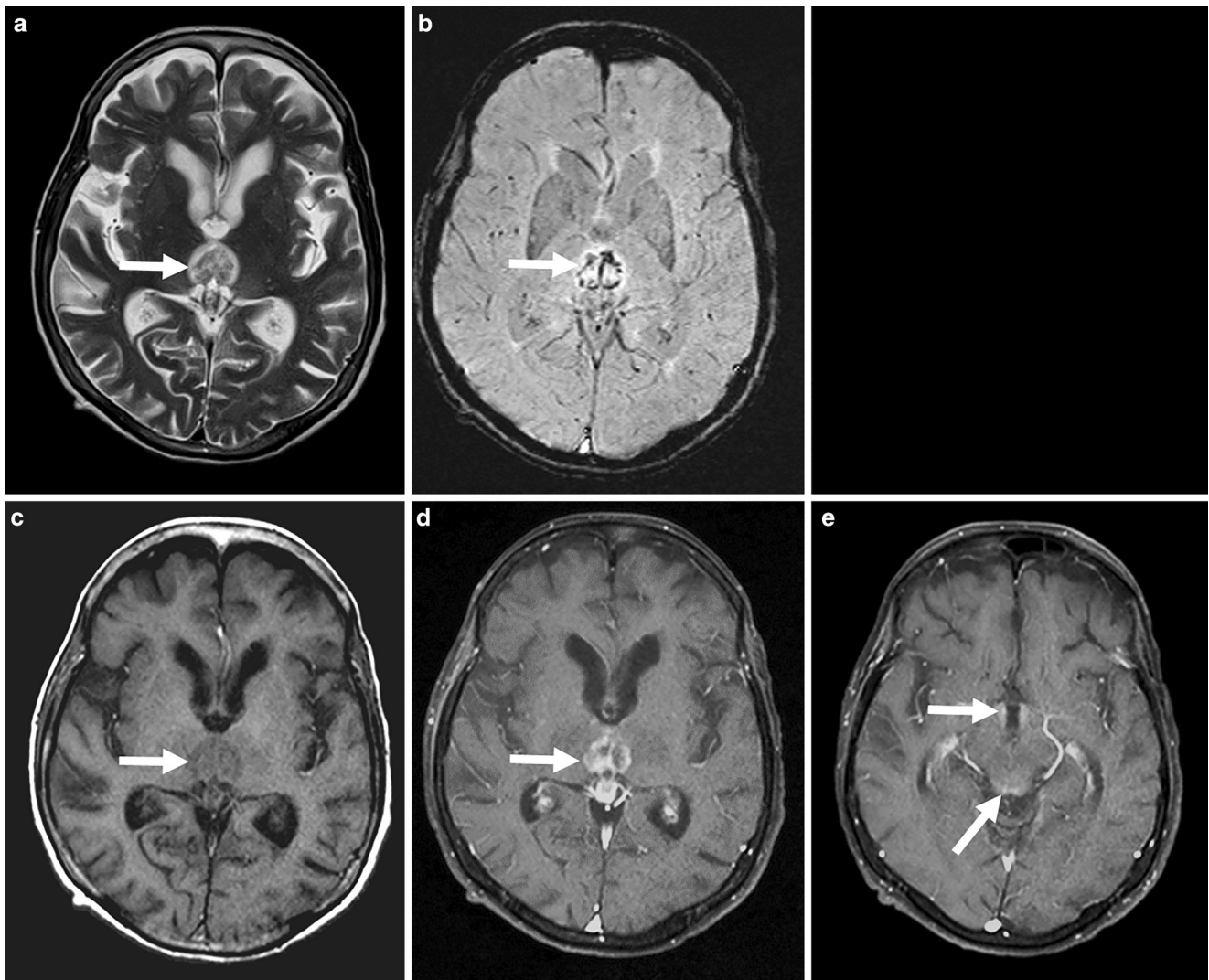
Fig. 10 Hemorrhagic transformation of affected paramedian thalamic nuclei in a 49-year-old female alcoholic with Wernicke encephalopathy. Inhomogeneous signal changes on axial T2-weighted images (WI) (**a**, arrow), punctuate signal loss on axial susceptibility-WI (**b**, arrow) and patchy enhancement on contrast-enhanced T1WI (**c** before, **d** after administration of contrast agent; arrow). Note additional enhancement of the hypothalamus and the quadrigeminal plate (**e**, arrows)

cranial nerve nuclei, respectively. In our cohort, only three patients were non-alcoholics with WE, one of whom did not reveal any atypical lesion site, while the other two cases presented involvement of the fornices. Most notably, this study first-ever described signal changes in the junction area of the mammillo-tegmental and habenulo-interpeduncular tracts, located just above the red nucleus [50], in a non-alcoholic young man who went on a hunger strike with consecutive thiamine deficiency. These changes were incompletely resolved on follow-up scans after intravenous substitution and resumed food intake (Fig. 4). Although the hippocampal formations play a central role in the medial limbic (Papez) circuit, crucial for memory storage, no one so far described MRI signal changes in this location. One exception was the study of Jordan et al. [51] using

quantitative T2 mapping, which revealed pathological alterations in the hippocampus formations and other regions in thiamine-deficient rats already 40 minutes following an additional glucose injection [51]. It should be emphasized that imaging techniques analyzing metabolic biomarkers, such as MRI combined with positron emission tomography [52, 53] or spectroscopy [54–57], may be more sensitive for in vivo detection of hippocampal involvement in WE, as neuronal loss may be not typically predominant in humans [58].

Parenchymal hemorrhage on T2*WI and SWI, with or without space-occupying vasogenic edema on T2WI and FLAIR, was an infrequent finding. Yet it remains unclear whether its count might have been higher if SWI had also been implemented in earlier MRI protocols. Besides the
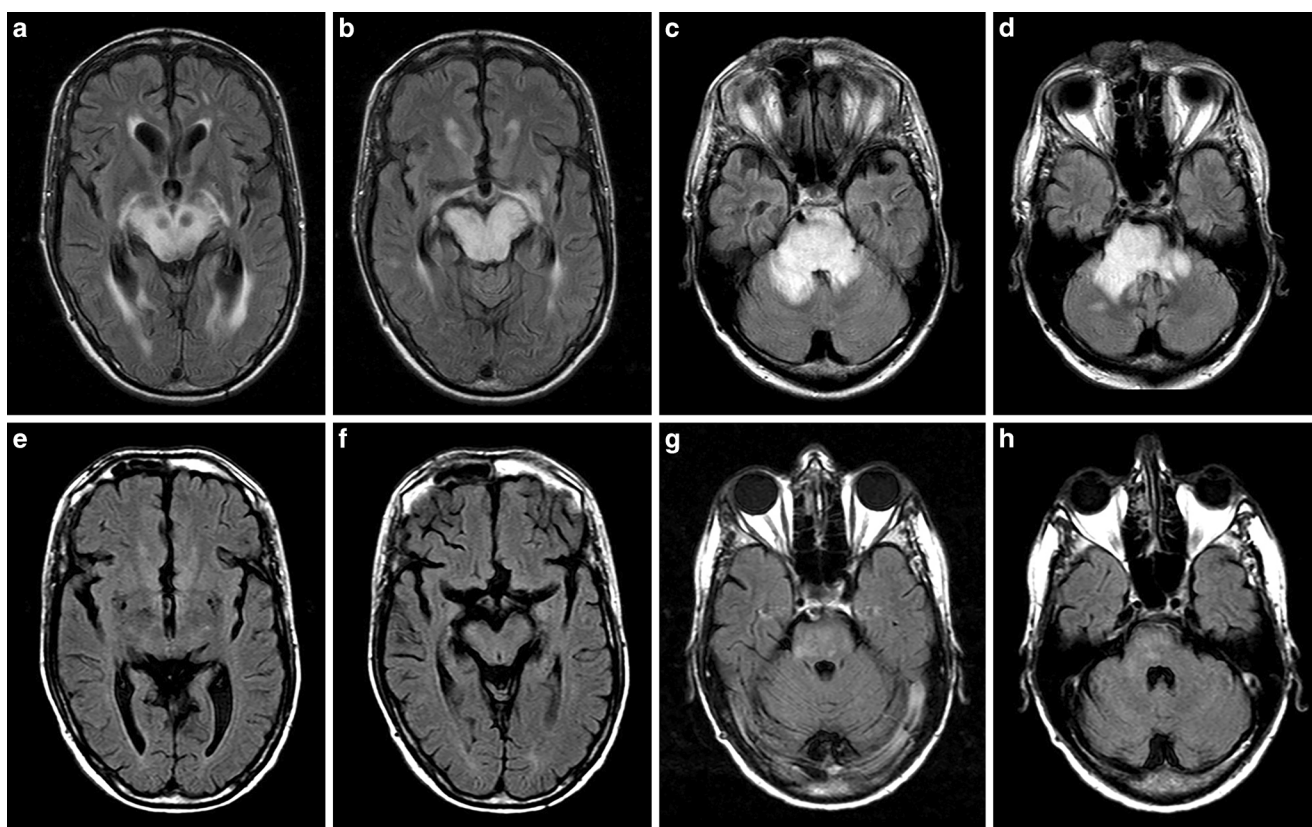
Fig. 11 **a–d** Extensive involvement of the optical pathway, internal capsule, brainstem and cerebellar peduncles in a 43-year-old male alcoholic suffering from acute Wernicke encephalopathy with hyperintense lesions on axial fluid-attenuated inversion recovery images. **e–h** Follow-up MRI 78 days later disclosed impressive lesion regression after intravenous vitamin B1 substitution, and neurological examination was unremarkable

more commonly described intra-axial hematomas in cortical and periventricular lesion sites found in autopsy studies [16], petechiae in the MB might be a more exceptional finding [3, 59, 60]. Our study cohort confirmed that petechial hemorrhage was confined to the MB, while larger collections of hemosiderin involved the periventricular regions. SWI was well-suited to detect these microbleeds in the MB and was clearly superior to simultaneously performed T2*WI (see Fig. 5) due to technical reasons. This is the first study to partially evaluate SWI and compare it to T2*WI in patients with WE. It underscores the practical value of hemosiderin-sensitive sequences in this cohort, which is not widely recognized, as it has only been described in a few case reports [17–19].

Atrophy of the MB was frequently detected in autopsy studies, especially in chronic forms of WE [61], but could also be found on MRI scans already within one week of acute symptom onset [30]. This study did not focus on a volumetric analysis of the involved brain structures. Semi-automated measurements of MB volumes using high-resolution T1WI might be a promising tool to increase the diagnostic sensitivity of standard MRI in patients suffering from WE, although they may not be very specific as even mild cognitive impairment has already shown significant differ-

ences compared to controls [62]. Other anatomical regions like the hippocampus formations, thalamus, pons, inferior colliculus, and cerebellum were also shown to be reduced in volumes in this patient cohort [30, 63, 64]. Park et al. demonstrated that alcoholics exhibited more pronounced atrophy of the superior vermis and MB, as well as enlargement of the third ventricle, compared to non-alcoholics [71].

In general, clinicians must be alert for WE due to the risk of permanent brain damage, such as the conversion into Korsakoff psychosis, or even death in cases where treatment with vitamin B1 was failed or delayed [65]. Recently, Silva et al. [66] indicated that the odds of having typical T2/FLAIR hyperintense changes decreased with increased doses of thiamine and earlier timing of supplementation. Therefore, when WE is suspected, thiamine should be immediately administered, preferably intravenously and before any carbohydrates [20]. Indeed, one of our patients experienced life-threatening bleeding induced by the intravenous administration of glucose prior to vitamin B1 (Fig. 9). Additionally, imaging studies showed that (1) the combined presence of cortical lesions and coma was associated with a poor prognosis [67], (2) signal changes in the medial thalamic nuclei on T2WI and in the MB on CE-T1WI were often related to irreversible amnesia [13,

Fig. 12 Normal and pathological periaqueductal grey appearance on axial fluid-attenuated inversion recovery images. **a** normal appearance on mid-lower level of the midbrain (**b**, MRI scout with corresponding intersection line) in a 47-year-old male healthy control, **c,d** pathological circular (**c**, arrow) and pathological wedge-shaped hyperintense signal changes of PAG (**d**, arrow) in a 46-year-old male alcoholic and a 64-year-old male alcoholic suffering from Wernicke encephalopathy, respectively
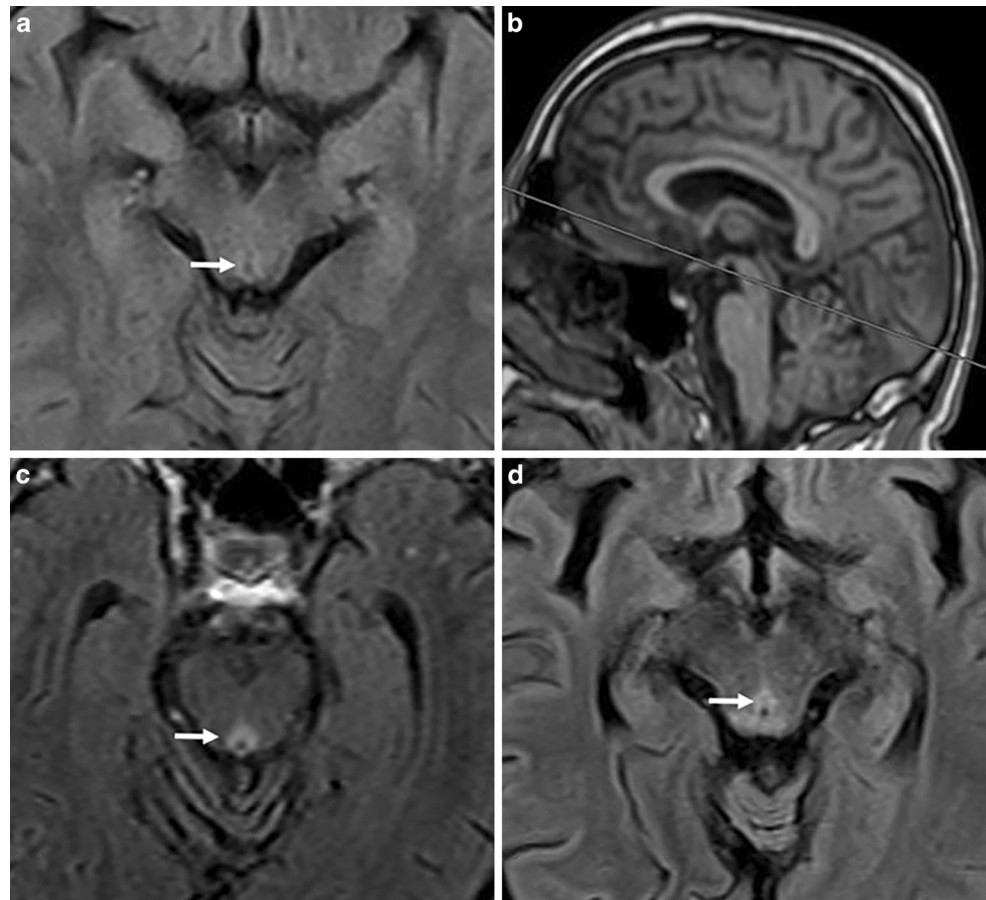
21, 30], and (3) case reports suggested a worse disease outcome when intra-axial hemorrhage was present [37, 68–70]. Lastly, it remains probable that the presence of MRI signal changes reflects the acute onset or an exacerbation of WE, such as cell swelling, demyelination, necrosis, vascular proliferation, disruption of the blood-brain barrier, and hemorrhage [15, 63, 71–73]. However, it remains unclear whether a certain imaging signature, like the onset of microbleeds or volume loss, might correctly classify the disease into

Table 2 Clinical features of 47 patients with diagnosed WE

Symptom	Numbers (%)
Oculomotor deficits	*36 (77)*
Abduction deficits	13 (28)
Gaze paresis	13 (28)
Nystagmus	31 (66)
Cognitive impairment/neuropsychological disturbances	*40 (85)*
Vigilance reduction	11 (23)
Orientation disturbances	25 (53)
Memory (short-term) deficits	19 (40)
Executive dysfunction (deceleration)	8 (17)
Cerebellar dysfunction	*40 (85)*
Ataxia	40 (85)

reversible or irreversible stages. Prospective analyses are lacking due to the many challenges present in this cohort.

Autopsy studies have revealed a range from 0.4 to 2.8% of prevalence for WE in the population, strongly suggesting that its diagnosis is greatly underreported [60, 74]. One probable reason might be the fact that only 16 to 33% of subjects present the classical triad of clinical symptoms [3]. Clinicians often face a diagnostic challenge due to the variable expression and broad range of neurological manifestations in a patient cohort that can be difficult to examine clinically, especially during episodes of more excessive alcohol consumption. The notably higher frequency of clinical signs in our cohort (oculomotor deficits, 77%; cognitive impairment/altered mental state, 85%; cerebellar dysfunction, 85%) might be attributed to the retrospective design of this study, which allowed local clinicians, particularly non-neurologists, to reevaluate differential diagnoses after image-guided suspicion of WE. Most interestingly, independent associations between imaging and clinical features could only be made for the presence of changes in the MB and memory impairment in our cohort, but not, as expected, for changes in/around the PAG and the tectal plate with oculomotor deficits, or in cerebellar regions with ataxia. Eventually, all subjects retrospectively met the 2010 EFNS criteria
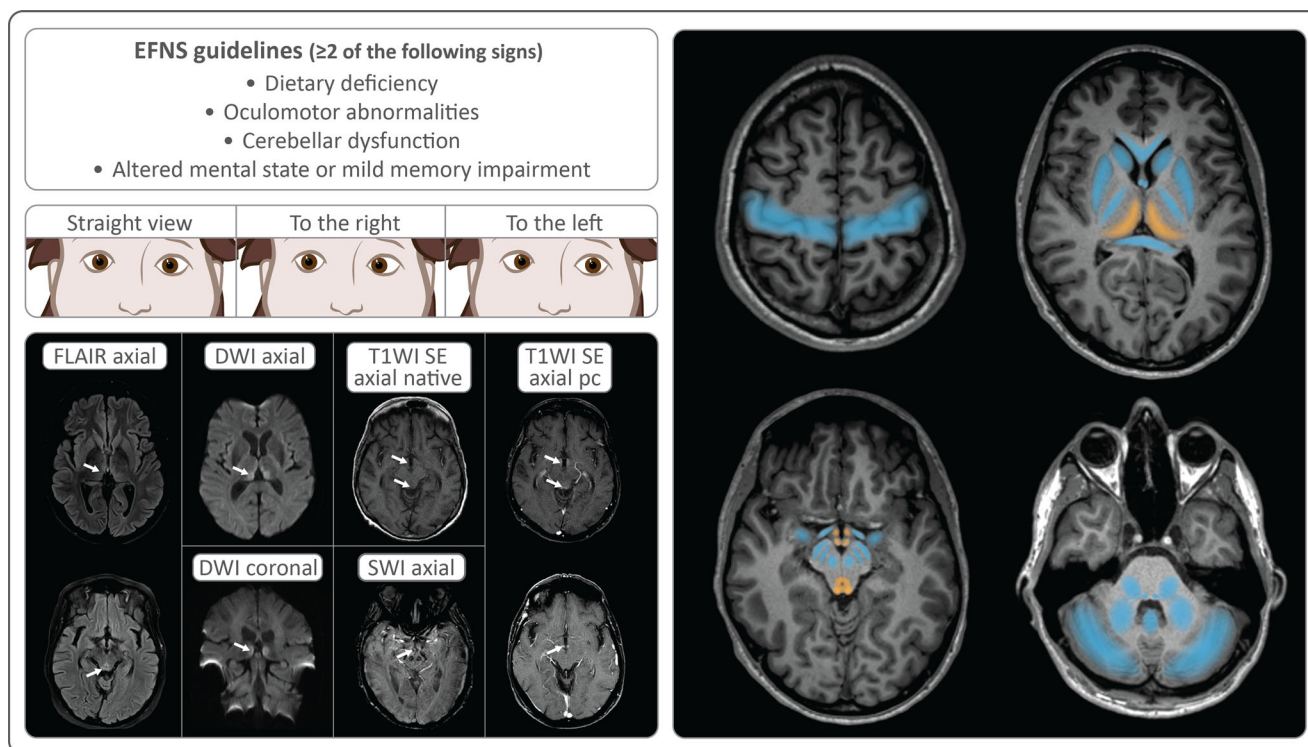
Fig. 13 Summary of clinical signs in Wernicke encephalopathy (WE) according to the latest European Federation of Neurological Societies (EFNS) guidelines and characteristic oculomotor abnormalities, i.e., bilateral abduction deficits. Proposed MRI sequences in WE disclosing signal changes in typical locations (medial thalamic nucleus, hypothalamus, mammillary body, periaqueductal grey and inferior colliculus of the quadrigeminal plate; marked in orange) and atypical locations (pre- and postcentral gyrus, basal ganglia, internal capsule, optic tract, fornix, amygdala, corpus callosum, red nucleus, substantia nigra, cerebral peduncle, cranial nerve nuclei, cerebellar peduncle, vermis, dentate nucleus, and cerebellar hemisphere; marked in blue). FLAIR, fluid-attenuated inversion recovery; DWI, diffusion-weighted imaging; pc, post-contrast; SE, spin echo; SWI, susceptibility-WI

[20]. However, it must be noted that this approach, which is based solely on the presence of a syndromic level, might trade lower specificity for very high sensitivity (e.g., dietary deficits in all chronic alcoholics). Furthermore, our study revealed no clear correlation between the number of positive EFNS criteria and the presence of imaging biomarkers. Excluding the rather unspecific measure of an inadequate supply of essential nutrients, two cases with only signs of cognitive impairment showed clear signal changes on MRI. To date, MRI is recommended to (only) support the diagnosis of WE in both alcoholics and non-alcoholics because it cannot be used to exclude the disease due to its reported rather low sensitivity of 53% [20, 22]. Our study revealed higher rates of positive imaging findings on standard MRI (77%), comparable to the results in studies by Zuccoli et al. (85 and 80%) [14, 30]. This could be explained not only by the analyses being performed by more experienced neuroradiologists, but also by the MRI protocols used in both radiology centers. Moreover, we are the first to describe an approach to manually measure the width of the PAG and set a reference range.

Besides increasing the diagnostic certainty by using the T2 shine-through phenomenon in b = 1000 DWI images or true diffusion restriction in ADC maps, another option to improve detection of hyperintense signal changes might be the implementation of a 3D T2WI and/or 3D FLAIR sequence in standard MRI protocols. However, attention must be paid to its pitfalls, especially in the more commonly involved infratentorial and deep grey matter structures. To overcome these technical hurdles, so-called FLAIR3 images, which can be reconstructed by combining both 3D FLAIR and 3D T2WI, might also enhance the depiction of hyperintense lesions [75]. Flow artifacts related to the cerebrospinal fluid (CSF) in the aqueduct could be a probable reason for the missing suppression of CSF, leading to surrounding small hyperintense signal changes (i.e., in the PAG) in 2D compared to 3D FLAIR images [76]. To account for this, we defined a cut-off value of 2.5 mm width for these hyperintense changes. In our patient cohort, 47% of cases showed 3–4 mm wide FLAIR-hyperintensities in the PAG, making it the second most involved location. Moreover, four patients were rated positive for WE only because these signal changes were detected in the PAG, underlining the importance of analyzing this region in MRI. Whereas in patients with relapsing-remitting multiple sclerosis and clinically isolated syndrome, round-shaped lesions

were more predominant than wedge-shaped ones (65 vs. 42%) [77], this study showed lower and opposite frequencies of involvement (11 vs. 32%), the latter possibly due to by the expansion to the neighboring tectum mesencephali. For the use of 3D gradient-echo T1WI, some relevant pitfalls may lead to a higher number of false positive results. Therefore, we recommend using 2D spin-echo CE-T1WI and comparing it with the native sequence. Generally, contrast enhancement in WE is predominantly observed in the MB and thalamus [30].

Finally, the aforementioned imaging findings are not specific for WE. Radiologists should consider several other conditions such as infarctions in the territory of the posterior thalamus-perforating arteries (artery of Percheron, in particular) [78], venous congestion from deep cerebral vein thrombosis or acute severe intracranial hypotension [79–81], infections and parainfectious acute disseminated encephalomyelitis [82–84], autoimmune diseases [77, 85–87], Creutzfeldt-Jakob disease and its variants [88], neoplasms [89–91] and metronidazole toxicity [92].

References

1. Wernicke C. Die akute, hämorrhagische Polioencephalitis superior. Lehrbuch der Gehirnkrankheiten für Aerzte und Studirende. 2nd ed. Berlin: Verlag von Theodor: Fischer; 1881. pp. 229–42.
2. Gayet CJA. Affection encéphalique (encéphalite diffuse probable). Localisée aux étages superieurs des pédoncles cérébraux et aux couches optiques, ainsi qu'ou plancher due quatrième ventricule et aux parois laterales du troisième. Observation recueillie. Arch De Physiol Norm Et Pathol. 1875;2(2):341–51.
3. Harper CG, Giles M, Finlay-Jones R. Clinical signs in the Wernicke-Korsakoff complex: a retrospective analysis of 131 cases diagnosed at necropsy. J Neurol Neurosurg Psychiatry. 1986;49(4):341–5. https://doi.org/10.1136/jnnp.49.4.341.
4. Kohnke S, Meek CL. Don't seek, don't find: The diagnostic challenge of Wernicke's encephalopathy. Ann Clin Biochem. 2021;58(1):38–46. https://doi.org/10.1177/0004563220939604.
5. Korsakoff SS. On alcoholic paralysis. Doctoral. Moscow: dissertation; 1877.
6. Kopelman MD, Thomson AD, Guerrini I, Marshall EJ. The Korsakoff syndrome: clinical aspects, psychology and treatment. alcohol Alcohol. 2009;44(2):148–54. https://doi.org/10.1093/alcalc/agn118.
7. Lana-Peixoto MA, Dos SEC, Pittella JE. Coma and death in unrecognized Wernicke's encephalopathy. An autopsy study. Arq Neuropsiquiatr. 1992;50(3):329–33. https://doi.org/10.1590/s0004-282x1992000300012.
8. Hazell AS, Todd KG, Butterworth RF. Mechanisms of neuronal cell death in Wernicke's encephalopathy. Metab Brain Dis. 1998;13(2):97–122. https://doi.org/10.1023/a:1020657129593.
9. Victor M, Adams RD, Collins GH. The Wernicke-Korsakoff syndrome. A clinical and pathological study of 245 patients, 82 with post-mortem examinations. Contemp Neurol Ser. 1971;7:1–206.
10. Victor M. The Wernicke-Korsakoff syndrome. In: Vinken PJ, Bruyn GW, editors. Handbook of clinical neurology. Vol. 28. Amsterdam: Elsevier; 1976. pp. 243–70.
11. Ota Y, Capizzano AA, Moritani T, Naganawa S, Kurokawa R, Srinivasan A. Comprehensive review of Wernicke encephalopathy: pathophysiology, clinical symptoms and imaging findings. Jpn J Radiol. 2020;38(9):809–20. https://doi.org/10.1007/s11604-020-00989-3.
12. Suzuki S, Ichijo M, Fujii H, Matsuoka Y, Ogawa Y. Acute Wernicke's encephalopathy: comparison of magnetic resonance images and autopsy findings. Intern Med. 1996;35(10):831–4. https://doi.org/10.2169/internalmedicine.35.831.
13. Zuccoli G, Pipitone N. Neuroimaging findings in acute Wernicke's encephalopathy: review of the literature. ajr Am J Roentgenol. 2009;192(2):501–8. https://doi.org/10.2214/AJR.07.3959.
14. Zuccoli G, Gallucci M, Capellades J, et al. Wernicke encephalopathy: MR findings at clinical presentation in twenty-six alcoholic and nonalcoholic patients. Ajnr Am J Neuroradiol. 2007;28(7):1328–31. https://doi.org/10.3174/ajnr.A0544.
15. Schroth G, Wichmann W, Valavanis A. Blood-brain-barrier disruption in acute Wernicke encephalopathy: MR findings. J Comput Assist Tomogr. 1991;15(6):1059–1061. https://doi.org/10.1097/00004728-199111000-00034
16. Rosenblum WI, Feigin I. The hemorrhagic component of Wernicke's encephalopathy. arch Neurol. 1965;13(6):627–32. https://doi.org/10.1001/archneur.1965.00470060063006.
17. Hattingen E, Beyle A, Müller A, Klockgether T, Kornblum C. Wernicke encephalopathy: SWI detects petechial hemorrhages in mammillary bodies in vivo. Neurology. 2016;87(18):1956–1957. https://doi.org/10.1212/WNL.0000000000003294
18. Weidauer S, Treusch N, Hattingen E. Petechial Hemorrhage in Wernicke Encephalopathy. Imaging Clin Significance clin Neuroradiol. 2022;32(1):309–12. https://doi.org/10.1007/s00062-021-01064-8.
19. Nakamura Y, Fushimi Y, Hinoda T, et al. Hemosiderin Detection inside the Mammillary Bodies Using Quantitative Susceptibility Mapping on Patients with Wernicke-Korsakoff Syndrome. Magn Reson Med Sci. Published online December 13, 2022. https://doi.org/10.2463/mrms.ici.2022-0109
20. Galvin R, Bråthen G, Ivashynka A, et al. EFNS guidelines for diagnosis, therapy and prevention of Wernicke encephalopathy. eur J Neurol. 2010;17(12):1408–18. https://doi.org/10.1111/j.1468-1331.2010.03153.x.
21. Weidauer S, Nichtweiss M, Lanfermann H, Zanella FE. Wernicke encephalopathy: MR findings and clinical presentation. Eur Radiol. 2003;13(5):1001–9. https://doi.org/10.1007/s00330-002-1624-7.
22. Antunez E, Estruch R, Cardenal C, Nicolas JM, Fernandez-Sola J, Urbano-Marquez A. Usefulness of CT and MR imaging in the diagnosis of acute Wernicke's encephalopathy. ajr Am J Roentgenol. 1998;171(4):1131–7. https://doi.org/10.2214/ajr.171.4.9763009.
23. Doss A, Mahad D, Romanowski CA. Wernicke encephalopathy: unusual findings in nonalcoholic patients. J Comput Assist Tomogr. 2003;27(2):235–40. https://doi.org/10.1097/00004728-200303000-00022.
24. Kang SY, Kang JH, Choi JC, Choi G. Wernicke's encephalopathy: unusual manifestation on MRI. J Neurol. 2005;252(12):1550–2. https://doi.org/10.1007/s00415-005-0886-9.
25. Bae SJ, Lee HK, Lee JH, Choi CG, Suh DC. Wernicke's encephalopathy: atypical manifestation at MR imaging. Ajnr Am J Neuroradiol. 2001;22(8):1480–2.
26. D'Aprile P, Tarantino A, Santoro N, Carella A. Wernicke's encephalopathy induced by total parenteral nutrition in patient with acute leukaemia: unusual involvement of caudate nuclei and cere-

bral cortex on MRI. Neuroradiology. 2000;42(10):781–3. https://doi.org/10.1007/s002340000393.

27. Zuccoli G, Motti L. Atypical Wernicke's encephalopathy showing lesions in the cranial nerve nuclei and cerebellum. J Neuroimaging. 2008;18(2):194–7. https://doi.org/10.1111/j.1552-6569.2007.00188.x.

28. Zuccoli G, Cravo I, Bailey A, Venturi A, Nardone R. Basal Ganglia involvement in Wernicke encephalopathy: report of 2 cases. AJNR Am J Neuroradiol. 2011;32(7):E

29. Sugai A, Kikugawa K. Atypical MRI findings of Wernicke encephalopathy in alcoholic patients. AJR Am J Roentgenol. 2010;195(5):W372–W374. https://doi.org/10.2214/AJR.10.4539.

30. Zuccoli G, Cruz SD, Bertolini M, et al. MR imaging findings in 56 patients with Wernicke encephalopathy: nonalcoholics may differ from alcoholics. AJNR Am J Neuroradiol. 2009;30(1):171–6. https://doi.org/10.3174/ajnr.A1280.

31. Eijkman C. Polyneuritis bij hoenders. Geneesk. tschr. Ned.-Indië. Band. 1890;30:295.

32. Oudman E, Wijnia JW, Oey MJ, van Dam M, Postma A. Wernicke-Korsakoff syndrome despite no alcohol abuse: A summary of systematic reports. J Neurol Sci. 2021;426:117482. https://doi.org/10.1016/j.jns.2021.117482.

33. Safran JT, Bodaghi M, Sherwin NK, Wallace JR. Wernicke's encephalopathy in adolescents with anorexia nervosa. Psychiatry Res Case Rep. 2023;2(1):100091. https://doi.org/10.1016/j.psycr.2022.100091

34. Weidauer S, Rösler A, Zanella FE, Lanfermann H. Diffusion-weighted imaging in Wernicke encephalopathy associated with stomach cancer: case report and review of the literature. Eur Neurol. 2004;51(1):55–7. https://doi.org/10.1159/000075093.

35. Wu L, Jin D, Sun X, et al. Cortical damage in Wernicke's encephalopathy with good prognosis: a report of two cases and literature review. Metab Brain Dis. 2017;32(2):377–84. https://doi.org/10.1007/s11011-016-9920-0.

36. Zhong C, Jin L, Fei G. MR Imaging of nonalcoholic Wernicke encephalopathy: a follow-up study. AJNR Am J Neuroradiol. 2005;26(9):2301–5.

37. Opdenakker G, Gelin G, De Surgeloose D, Palmers Y. Wernicke encephalopathy: MR findings in two patients. Eur Radiol. 1999;9(8):1620–4. https://doi.org/10.1007/s003300050896.

38. Ramineni KK, Marupaka SK, Jakkani R, Ingle A. Wernicke Encephalopathy with Atypical Findings on Magnetic Resonance Imaging. Ann Indian Acad Neurol. 2018;21(4):328–30. https://doi.org/10.4103/aian.AIAN_65_18.

39. Hernández MA, Varela F, Bensi C. Optic tract and internal capsule lesion in a patient with Wernicke-Korsakoff syndrome: Lesión del tracto óptico y de la cápsula interna en un paciente con síndrome de Wernicke-Korsakoff. J Appl Cogn Neurosci. 2020;1(1):101–103.

40. Loh Y, Watson WD, Verma A, Krapiva P. Restricted diffusion of the splenium in acute Wernicke's encephalopathy. J Neuroimaging. 2005;15(4):373–5. https://doi.org/10.1177/1051228405279037.

41. Desai SD, Shah DS. Atypical Wernicke's syndrome sans encephalopathy with acute bilateral vision loss due to post-chiasmatic optic tract edema. Ann Indian Acad Neurol. 2014;17(1):103–5. https://doi.org/10.4103/0972-2327.128567i.

42. Mackay CJ, Tran VT, Chen Y. Optic Chiasm Involvement With Concurrent Typical Wernicke Encephalopathy Magnetic Resonance Findings: A Case Report. Curr Probl Diagn Radiol. 2018;47(6):452–5. https://doi.org/10.1067/j.cpradiol.2017.09.004.

43. Swenson AJ, Louis StEK. Computed tomography findings in thiamine deficiency-induced coma. Neurocrit Care. 2006;5(1):45–8. https://doi.org/10.1385/ncc:5:1:45.

44. Bonucchi J, Hassan I, Policeni B, Kaboli P. Thyrotoxicosis associated Wernicke's encephalopathy. J Gen Intern Med. 2008;23(1):106–9. https://doi.org/10.1007/s11606-007-0438-3.

45. Kalidass B, Sunnathkal R, Rangashamanna DV, Paraswani R. Atypical Wernicke's encephalopathy showing involvement of substantia nigra. J Neuroimaging. 2012;22(2):204–7. https://doi.org/10.1111/j.1552-6569.2010.00545.x.

46. Nolli M, Barbieri A, Pinna C, Pasetto A, Nicosia F. Wernicke's encephalopathy in a malnourished surgical patient: clinical features and magnetic resonance imaging. Acta Anaesthesiol Scand. 2005;49(10):1566–70. https://doi.org/10.1111/j.1399-6576.2005.00879.x.

47. Ghorbani A, Fatehi F, Soltanzadeh A, Hamidieh A, Vahabi Z. Wernicke's Encephalopathy in a Young Girl Suffering from Acute Myeloblastic Leukemia. Iran J Pediatr. 2012;22(4):574–575.i

48. Lapergue B, Klein I, Olivot JM, Amarenco P. Diffusion weighted imaging of cerebellar lesions in Wernicke's encephalopathy. J Neuroradiol. 2006;33(2):126–128. https://doi.org/10.1016/s0150-9861(06)77243-1

49. Kim JE, Kim TH, Yu IK, Lee BR, Lee SJ, Oh GS. Diffusion-Weighted MRI in Recurrent Wernicke's Encephalopathy: a Remarkable Cerebellar Lesion. J Clin Neurol. 2006;2(2):141–5. https://doi.org/10.3988/jcn.2006.2.2.141.

50. Nieuwenhuys R, Voogd J, van Huijzen C. Das Zentralnervensystem des Menschen: Ein Atlas mit Begleittext. 2nd. Ed Berlin: Springer-verlag. 1991;311.

51. Jordan LR, Zelaya FO, Rose SE, et al. Changes in the hippocampus induced by glucose in thiamin deficient rats detected by MRI. Brain Res. 1998;791(1–2):347–351. https://doi.org/10.1016/s0006-8993(98)00203-0

52. Rozenblum L, Habert MO, Pyatigorskaya N, Roue-Jagot C, Kas A. FDG PET/MRI Findings Pointing Toward a Gayet-Wernicke Encephalopathy. Clin Nucl Med. 2019;44(7):e456–e7. https://doi.org/10.1097/RLU.0000000000002601.

53. Reed LJ, Lasserson D, Marsden P, et al. FDG-PET findings in the Wernicke-Korsakoff syndrome. Cortex. 2003;39(4–5):1027–1045. https://doi.org/10.1016/s0010-9452(08)70876-1

54. Murata T, Fujito T, Kimura H, Omori M, Itoh H, Wada Y. Serial MRI and (1)H-MRS of Wernicke's encephalopathy: report of a case with remarkable cerebellar lesions on MRI. Psychiatry Res. 2001;108(1):49–55. https://doi.org/10.1016/s0925-4927(01)00304-3

55. Rodan LH, Mishra N, Tein I. MR spectroscopy in pediatric Wernicke encephalopathy. Neurology. 2013;80(10):969. https://doi.org/10.1212/WNL.0b013e3182840cd9.

56. Mascalchi M, Belli G, Guerrini L, Nistri M, Del Seppia I, Villari N. Proton MR spectroscopy of Wernicke encephalopathy. AJNR Am J Neuroradiol. 2002;23(10):1803–6.

57. Rugilo CA, Uribe Roca MC, Zurru MC, Capizzano AA, Pontello GA, Gatto EM. Proton MR spectroscopy in Wernicke encephalopathy. AJNR Am J Neuroradiol. 2003;24(5):952–5.

58. Harding AJ, Wong A, Svoboda M, Kril JJ, Halliday GM. Chronic alcohol consumption does not cause hippocampal neuron loss in humans. Hippocampus. 1997;7(1):78–87. https://doi.org/10.1002/(SICI)1098-1063(1997)7:1⟨78::AID-HIPO8⟩3.0.CO;2-3

59. Hata Y, Takeuchi Y, Kinoshita K, Nishida N. An autopsy case of acute and nonalcoholic thiamine-deficient encephalopathy. Eur Neurol. 2014;71(5–6):230–232. https://doi.org/10.1159/000354185

60. Harper C. The incidence of Wernicke's encephalopathy in Australia—a neuropathological study of 131 cases. J Neurol Neurosurg Psychiatry. 1983;46(7):593–8. https://doi.org/10.1136/jnnp.46.7.593.

61. Sheedy D, Lara A, Garrick T, Harper C. Size of mamillary bodies in health and disease: useful measurements in neuroradiological diagnosis of Wernicke's encephalopathy. Alcohol Clin Exp Res. 1999;23(10):1624–8.

62. Jin Z, Sethi SK, Li B, et al. Susceptibility and Volume Measures of the Mammillary Bodies Between Mild Cognitively Impaired Pa-

tients and Healthy Controls. Front Neurosci. 2020;14:572595. Published 2020 Sep 15. https://doi.org/10.3389/fnins.2020.572595

63. Sullivan EV, Pfefferbaum A. Neuroimaging of the Wernicke-Korsakoff syndrome. Alcohol Alcohol. 2009;44(2):155–65. https://doi.org/10.1093/alcalc/agn103.

64. Bordia T, Zahr NM. The Inferior Colliculus in Alcoholism and Beyond. Front Syst Neurosci. 2020;14:606345. Published 2020 Dec 11. https://doi.org/10.3389/fnsys.2020.606345

65. Donnino MW, Vega J, Miller J, Walsh M. Myths and misconceptions of Wernicke's encephalopathy: what every emergency physician should know. Ann Emerg Med. 2007;50(6):715–21. https://doi.org/10.1016/j.annemergmed.2007.02.007.

66. Silva AR, Almeida-Xavier S, Lopes M, Soares-Fernandes JP, Sousa F, Varanda S. Is there a time window for MRI in Wernicke encephalopathy—a decade of experience from a tertiary hospital. Neurol Sci. 2023;44(2):703–8. https://doi.org/10.1007/s10072-022-06477-y.

67. Fei GQ, Zhong C, Jin L, et al. Clinical characteristics and MR imaging features of nonalcoholic Wernicke encephalopathy. AJNR Am J Neuroradiol. 2008;29(1):164–9. https://doi.org/10.3174/ajnr.A0827.

68. DePolo D, Gillen S, Marden K, et al. Severe Wernicke's Encephalopathy Associated with Cortical Ribboning and Intracranial Hemorrhage. Neurohospitalist. 2022;12(4):702–5. https://doi.org/10.1177/19418744221098385.

69. Al-Bayati AR, Nichols J, Jovin TG, Jadhav AP. Thiamine Deficiency Presenting as Intraventricular Hemorrhage. Stroke. 2016;47(6):e95–e7. https://doi.org/10.1161/STROKEAHA.116.013048.

70. Jeon S, Kang H. Wernicke's Encephalopathy with Intracranial Hemorrhage. Investig Magn Reson Imaging. 2016;20(1):71–4. https://doi.org/10.13104/imri.2016.20.1.71.

71. Park SH, Kim M, Na DL, Jeon BS. Magnetic resonance reflects the pathological evolution of Wernicke encephalopathy. J Neuroimaging. 2001;11(4):406–11. https://doi.org/10.1111/j.1552-6569.2001.tb00070.x.

72. Liu YT, Fuh JL, Lirng JF, Li AF, Ho DM, Wang SJ. Correlation of magnetic resonance images with neuropathology in acute Wernicke's encephalopathy. Clin Neurol Neurosurg. 2006;108(7):682–7. https://doi.org/10.1016/j.clineuro.2005.05.010.

73. Gui QP, Zhao WQ, Wang LN. Wernicke's encephalopathy in nonalcoholic patients: clinical and pathologic features of three cases and literature reviewed. Neuropathology. 2006;26(3):231–5. https://doi.org/10.1111/j.1440-1789.2006.00665.x.

74. Harper C, Fornes P, Duyckaerts C, Lecomte D, Hauw JJ. An international perspective on the prevalence of the Wernicke-Korsakoff syndrome. Metab Brain Dis. 1995;10(1):17–24. https://doi.org/10.1007/BF01991779.

75. Gabr RE, Lincoln JA, Kamali A, et al. Sensitive Detection of Infratentorial and Upper Cervical Cord Lesions in Multiple Sclerosis with Combined 3D FLAIR and T2-Weighted (FLAIR3) Imaging. Ajnr Am J Neuroradiol. 2020;41(11):2062–7. https://doi.org/10.3174/ajnr.A6797.

76. Naganawa S, Koshikawa T, Nakamura T, et al. Comparison of flow artifacts between 2D-FLAIR and 3D-FLAIR sequences at 3 T. Eur Radiol. 2004;14(10):1901–8. https://doi.org/10.1007/s00330-004-2372-7.

77. Papadopoulou A, Naegelin Y, Weier K, et al. MRI characteristics of periaqueductal lesions in multiple sclerosis. Mult Scler Relat Disord. 2014;3(4):542–51. https://doi.org/10.1016/j.msard.2014.01.001.

78. Weidauer S, Nichtweiss M, Zanella FE, Lanfermann H. Assessment of paramedian thalamic infarcts: MR imaging, clinical features and prognosis. Eur Radiol. 2004;14(9):1615–26. https://doi.org/10.1007/s00330-004-2303-7.

79. Caplan LR, Wang Q. Thalamic Lesions Caused by Deep Cerebral Venous Thrombosis: A Retrospective Study. Eur Neurol. 2015;74(1–2):118–126. https://doi.org/10.1159/000439167

80. Lachner K, You SJ, Konczalla J, Hattingen E, Czabanka M, Weidauer S. Postoperative intracranial hypotension-associated venous congestion: the lentiform rim sign [Postoperative intrakranielle unterdruckassoziierte venöse Kongestion: das „lentiform rim sign"]. Rofo. 2023;195(10):924–926. https://doi.org/10.1055/a-2066-8059

81. Van Roost D, Thees C, Brenke C, Oppel F, Winkler PA, Schramm J. Pseudohypoxic brain swelling: a newly defined complication after uneventful brain surgery, probably related to suction drainage. Neurosurgery. 2003;53(6):1315–27. https://doi.org/10.1227/01.neu.0000093498.08913.9e.

82. Beattie GC, Glaser CA, Sheriff H, et al. Encephalitis with thalamic and basal ganglia abnormalities: etiologies, neuroimaging, and potential role of respiratory viruses. Clin Infect Dis. 2013;56(6):825–32. https://doi.org/10.1093/cid/cis990.

83. Zheng Y, Zhang W, Hao H, Gao F. Bilateral thalamic lesions in a patient with probable acute disseminating encephalomyelitis: a case report. BMC Neurol. 2020;20(1):265. Published 2020 Jul 1. https://doi.org/10.1186/s12883-020-01834-w

84. Gupta RK, Soni N, Kumar S, Khandelwal N. Imaging of central nervous system viral diseases. J Magn Reson Imaging. 2012;35(3):477–91. https://doi.org/10.1002/jmri.22830.

85. Ye L, Xu Z, Deng J, Yang J. Classical Triad and Periventricular Lesions Do Not Necessarily Indicate Wernicke's Encephalopathy: A Case Report and Review of the Literature. Front Neurol. 2020;11:451. Published 2020 Jun 10. https://doi.org/10.3389/fneur.2020.00451

86. Dalmau J, Graus F, Villarejo A, et al. Clinical analysis of anti-Ma2-associated encephalitis. Brain. 2004;127(Pt 8):1831–1844. https://doi.org/10.1093/brain/awh203.

87. Shan F, Zhong R, Wu L, Fan Y, Long Y, Gao C. Neuromyelitis optica spectrum disorders may be misdiagnosed as Wernicke's encephalopathy. Int J Neurosci. 2016;126(10):922–7. https://doi.org/10.3109/00207454.2015.1084619.

88. Nafe R, Arendt CT, Hattingen E. Human prion diseases and the prion protein—what is the current state of knowledge?. Transl Neurosci. 2023;14(1):20220315. Published 2023 Oct 16. https://doi.org/10.1515/tnsci-2022-0315

89. Brechtelsbauer DL, Urbach H, Sommer T, Blümcke I, Woitas R, Solymosi L. Cytomegalovirus encephalitis and primary cerebral lymphoma mimicking Wernicke's encephalopathy. Neuroradiology. 1997;39(1):19–22. https://doi.org/10.1007/s002340050359.

90. Yaldizli O, Wurst FM, Euler S, Willi B, Wiesbeck G. Multiple cerebral metastases mimicking Wernicke's encephalopathy in a chronic alcoholic. Alcohol Alcohol. 2006;41(6):678–80. https://doi.org/10.1093/alcalc/agl054.

91. Wu L, Jin D, Huang D, Yu S. Primary Central Nervous System Lymphoma Mimicking Wernicke's Encephalopathy. Neurol India. 2021;69(3):740–3. https://doi.org/10.4103/0028-3886.319202.

92. Kim E, Na DG, Kim EY, Kim JH, Son KR, Chang KH. MR imaging of metronidazole-induced encephalopathy: lesion distribution and diffusion-weighted imaging findings. Ajnr Am J Neuroradiol. 2007;28(9):1652–8. https://doi.org/10.3174/ajnr.A0655.